Diamagnetic shift and oscillator strength of two-dimensional excitons under a magnetic field in $In_{0.53}Ga_{0.47}As/InP$ quantum wells

Mitsuru Sugawara, Niroh Okazaki, Takuya Fujii, and Susumu Yamazaki
Fujitsu Laboratories Ltd., 10-1 Morinosato-Wakamiya, Atsugi 243-01, Japan
(Received 22 February 1993; revised manuscript received 20 May 1993)

We studied magneto-optical absorption spectra of the ground-state electron-heavy-hole exciton resonance in $In_{0.53}Ga_{0.47}As/InP$ quantum wells. As the magnetic field perpendicular to the quantum-well layers was increased, the exciton resonance showed diamagnetic shifts and its integrated intensity increased. Magneto-optical data were analyzed using effective-mass equations which include conduction- and valence-subband nonparabolic dispersion and the wave-vector dependent transition-matrix element with the second-order $\mathbf{k}\cdot\mathbf{p}$ terms. We found that the exciton wave function for the relative in-plane motion shrinks in real space and expands in k space due to the in-plane parabolic confinement potential by the magnetic fields. This enhanced the integrated intensity and thus, the oscillator strength. We evaluated the exciton reduced effective mass, Luttinger-Kohn valence-band effective-mass parameters, conduction-band effective mass, and a momentum matrix element between s- and p-state band-edge basis functions.

I. INTRODUCTION

Two-dimensional Wannier excitons under magnetic fields were first theoretically studied by Akimoto and Hasegawa in 1967.[1] Using two-dimensional effective-mass equations, they calculated diamagnetic shifts and oscillator strengths in the direct-allowed exciton resonance as a function of the magnetic field. Later in 1984, the magneto-optical effect on two-dimensional excitons was experimentally studied by Miura[2] and Maan[3] using $GaAs/Al_xGa_{1-x}As$ quantum wells. Since then, the exciton diamagnetic shift in GaAs quantum-well systems has been extensively studied,[4-13] giving us important information on two-dimensional exciton characteristics such as binding energy and reduced effective mass. The oscillator strength of the exciton resonance under a magnetic field, however, has received little attention. Previously, using 10-nm $In_{0.53}Ga_{0.47}As/InP$ quantum wells, we evaluated the integrated intensity of optical-absorption spectra of the electron-heavy-hole (HH) exciton resonance as a function of the magnetic field of up to 8 T.[14] (Since the integrated intensity is evaluated directly from optical-absorption data, we used it rather than the oscillator strength to represent the strength of the exciton resonance.) We demonstrated that the oscillator strength, which is proportional to the integrated intensity, increased with the magnetic field due to the field-induced shrinkage of the exciton in-plane relative-motion wave function.

Our theoretical analyses of the magneto-optical data left some unsatisfactory disagreements with the measurements, however. The measured diamagnetic shifts gradually separated downward from the calculated curve in the high magnetic-field region and the integrated intensity gradually separated upward. The exciton reduced effective mass obtained from the diamagnetic shift was $\mu=0.035m_0-0.04m_0$ and the mass which explained the integrated intensity was $\mu=0.04m_0-0.05m_0$, showing a definite discrepancy (see Figs. 2 and 4 in Ref. 14). We presumed that these disagreements were due to our simple theoretical model assuming parabolic band dispersion and using the band-edge matrix element given by the first-order $\mathbf{k}\cdot\mathbf{p}$ perturbation.

In this work we have studied exciton optical-absorption spectra under magnetic fields in lattice-matched $In_{0.53}Ga_{0.47}As/InP$ quantum wells, taking into account conduction- and valence-subband nonparabolic dispersion and using the wave-vector-dependent transition-matrix element with the second-order $\mathbf{k}\cdot\mathbf{p}$ term. First, we incorporate these effects to exciton effective-mass equations which we used previously. We evaluated three quantum-well samples with different well widths to avoid experimental errors. We observed both diamagnetic shifts and the enhancement of integrated intensity in the ground-state electron-HH exciton resonance under magnetic fields perpendicular to quantum-well layers. We could explain both the diamagnetic shifts and integrated intensity quite excellently for all samples, having confirmed our previous conclusion. We evaluated exciton reduced effective mass, Luttinger-Kohn valence-band effective-mass parameters, conduction-band effective mass, and a momentum matrix element between s- and p-state band-edge basis functions.

II. EXCITON EFFECTIVE-MASS EQUATIONS IN QUANTUM WELLS UNDER MAGNETIC FIELD

The influence of a magnetic field on exciton wave functions is determined by the ratio of the cyclotron energy of electrons and holes, $\hbar\omega_c=e\hbar B/\mu$, and the exciton binding energy E_b, i.e., $\xi=\hbar\omega_c/2E_b$, where $-e$ is the electron charge, $\hbar$ is Planck's constant divided by 2π, B is the magnetic-field strength, and μ is the reduced effective mass.[15] In the low-field limit of $\xi\ll 1$, the magnetic field

only perturbs exciton states, hardly changing their wave functions. We need a magnetic-field strength for a ratio of at least $\xi=1$. In $In_{0.53}Ga_{0.47}As/InP$ quantum wells, using $\mu=0.04m_0$ and $E_b=-6.6$ meV,[16] we obtain $\xi=1$ at 4.6 T. In our experiments, we applied magnetic fields of 0–8 T ($\xi=0-1.8$). We will describe exciton effective-mass equations in quantum wells treating both Coulomb potential energy and magnetic-field energy equally. In the high-field limit of $\xi\gg1$, where electrons and holes are under cyclotron motion and perturbation from Coulomb interaction generates bound states belonging to Landau levels, we can use the conventional treatment of Landau states.

A. Diamagnetic shift

Using an effective-mass approximation, we examine exciton states in zinc-blende direct-gap semiconductor quantum wells grown on (001) substrates. The wave function is the linear combination of the product of a free electron and a hole state,[15,17,18]

$$\Psi=\sum_{\mathbf{k}_e,\mathbf{k}_h} A_{nm}(\mathbf{k}_e,\mathbf{k}_h)|n,\mathbf{k}_e\rangle|m,\mathbf{k}_h\rangle\ , \tag{1}$$

where

$$|n,\mathbf{k}_e\rangle=\sqrt{\Omega/D}\,e^{i\mathbf{k}_e\cdot\mathbf{r}_e}\sum_j \varphi^j_{e,n}(z_e,\mathbf{k}_e)u^j_{c,0} \tag{2}$$

is the wave function of an electron and

$$|m,\mathbf{k}_h\rangle=\sqrt{\Omega/D}\,e^{i\mathbf{k}_h\cdot\mathbf{r}_h}\sum_j \varphi^j_{h,m}(z_h,\mathbf{k}_h)u^j_{v,0} \tag{3}$$

is that of a hole. Here, Ω is the unit-cell volume, D is the area of quantum wells, $\mathbf{k}_e$ and $\mathbf{k}_h$ are the in-plane wave vectors, $\mathbf{r}_e$ and $\mathbf{r}_h$ are the in-plane coordinate vectors, z_e and z_h are the coordinates in the direction perpendicular to the quantum-well layers, n is the quantum number describing confined states in the conduction band, m is that in the valence band, and $\varphi^j_{e,n}$ and $\varphi^j_{h,m}$ are confined-state wave functions. The periodic parts of band-edge Bloch functions (normalized in the unit cell) of the electron state, $u^j_{c,0}$, are primarily composed of s-state functions.[19] For those of the hole state, $u^j_{v,0}$, we use p-state functions which diagonalize spin-orbit interaction in the (J,M_J) representation.[19,20]

Neglecting the mixing of band-edge characters in Eqs. (2) and (3), Eq. (1) becomes

$$\Psi=\frac{\Omega}{D}\sum_{\mathbf{k}_\parallel} A_n(\mathbf{k}_\parallel)e^{i\mathbf{k}_\parallel\cdot\mathbf{r}}\varphi_{e,n}(z_e)\varphi_{h,n}(z_h)u_{c,0}u_{v,0}\ , \tag{4}$$

where $\mathbf{r}=\mathbf{r}_e-\mathbf{r}_v$ is the in-plane electron-hole distance. This is a good approximation since the expansion coefficient in Eq. (1), $A_{nm}(\mathbf{k}_e,\mathbf{k}_h)$, rapidly decreases as the wave vectors increase and the exciton state consists primarily of near-band-edge states [see Eq. (9) below]. In this way, excitons are classified by their band-edge characters, for example, electron-HH excitons for $u_{c,0}=|s,\uparrow\rangle$, $u_{v,0}=|\frac{3}{2},+\frac{3}{2}\rangle$ and $u_{c,0}=|s,\downarrow\rangle$, $u_{v,0}=|\frac{3}{2},-\frac{3}{2}\rangle$. We included the in-plane wave-vector selection rule as $\mathbf{k}_e=-\mathbf{k}_h=\mathbf{k}_\parallel$ under the electric-dipole approximation, and that of the confined-state wave function as $n=m$, for the interband optical transition. The former wave-vector selection rule requires $\mathbf{K}=\mathbf{0}$, where $\mathbf{K}$ is the in-plane wave vector of the exciton center of mass.

The exciton resonance energy in quantum wells under magnetic fields perpendicular to quantum-well layers is

$$E_{\rm ex}=E_A+E^z_{e,n}+E^z_{h,n}+E_r+E_{\rm sp}\ , \tag{5}$$

where E_A is the band gap of well materials, $E^z_{e,n}$ is the confined-state energy in the conduction band, and $E^z_{h,n}$ is that in the valence band. Equation (5) holds if the Coulomb interaction is weak compared with the quantum confinement potentials, and the confined-state wave functions are not perturbed. Under the z-direction magnetic field B, the spin-splitting energy is given as $E_{\rm sp}=\pm\mu_B\nu B$ (+ for $M_J=\frac{3}{2}$ and $\frac{1}{2}$ and − for $M_J=-\frac{3}{2}$ and $-\frac{1}{2}$), where $\mu_B=e\hbar/2m_0$, $\nu=g_e/2-3\kappa-27q/4$ for electron-HH exciton, $\nu=\pm g_e/2-\kappa-q/4$ for electron-light-hole (LH) exciton, g_e is the g factor of the conduction-band electron, and κ and q are Luttinger-Kohn valence-band parameters.[21] Since we observed no spin splitting of the exciton resonance (Sec. IV and Ref. 14), we neglect $E_{\rm sp}$. For parabolic band dispersion, E_r is the eigenvalue of the following effective-mass equation[17]:

$$\left[-\frac{\hbar^2}{2\mu}\nabla^2_{\mathbf{r}}-\frac{e^2}{4\pi\varepsilon\rho}-ie\hbar(m_e^{\parallel-1}-m_h^{\parallel-1})\mathbf{A}_p\cdot\nabla+\frac{e^2A_p^2}{2\mu}\right]\psi_{\rm env}=E_r\psi_{\rm env}\ , \tag{6}$$

where $\mu=(m_e^{\parallel-1}+m_h^{\parallel-1})^{-1}$ is the in-plane reduced effective mass, $m_e^\parallel$ is the in-plane electron effective mass, $m_h^\parallel$ is the in-plane hole effective mass, $\rho=[r^2+(z_e-z_h)^2]^{1/2}$, and ε is the static dielectric constant. The vector potential is taken as $\mathbf{A}_p=\mathbf{B}\times\mathbf{r}/2$. The envelope wave function is

$$\psi_{\rm env}=\frac{1}{\sqrt{D}}\phi_{\rm ex}(\mathbf{r})\varphi_{e,n}(z_e)\varphi_{h,n}(z_h)=\frac{1}{D}\sum_{\mathbf{k}_\parallel}A_n(\mathbf{k}_\parallel)e^{i\mathbf{k}_\parallel\cdot\mathbf{r}}\varphi_{e,n}(z_e)\varphi_{h,n}(z_h)\ , \tag{7}$$

where $\phi_{\rm ex}(\mathbf{r})$ represents the in-plane relative motion of an electron and a hole. Since the oscillator strength of a single-photon optical absorption is proportional to $|\phi_{\rm ex}(0)|^2$ (Refs. 22 and 23) and only s-state excitons are allowed in direct transitions, we take the linear combination of the hydrogenic and harmonic-oscillator s-state wave functions[13]

$$\phi_{\rm ex}(\mathbf{r})=\sqrt{2/\pi}\left[\frac{a}{\lambda}e^{-r/\lambda}+\frac{b}{\eta}e^{-r^2/\eta^2}\right]\ , \tag{8}$$

where λ, η, a, and b are variational parameters. Three of them are independent, and are determined to minimize exciton energy. While the hydrogenic function describes exciton states at zero field,[24,25] the harmonic-oscillator function becomes dominant as the magnetic field increases.[13] The expansion coefficient describing exciton

states in Eq. (4) is the Fourier transform of the in-plane envelope wave function, and is given as

$$A_n(\mathbf{k}_\parallel)=\frac{1}{\sqrt{D}}\int d^2\mathbf{r}\, e^{-i\mathbf{k}_\parallel\cdot\mathbf{r}}\phi_{\rm ex}(\mathbf{r})$$
$$=\sqrt{2\pi/D}\left[\frac{2\lambda a}{(1+k_\parallel^2\lambda^2)^{3/2}}+\eta b e^{-\eta^2 k_\parallel^2/4}\right]. \quad (9)$$

For s-state excitons under a magnetic field perpendicular to the quantum-well layers, Eq. (6) becomes

$$E_r=\left\langle\psi_{\rm env}\left|-\frac{\hbar^2}{2\mu}\left(\frac{\partial^2}{\partial r^2}+\frac{1}{r}\frac{\partial}{\partial r}\right)-\frac{e^2}{4\pi\varepsilon\rho}\right.\right.$$
$$\left.\left.+\frac{e^2B^2}{8\mu}r^2\right|\psi_{\rm env}\right\rangle. \quad (10)$$

The third term in Eq. (10) is the diamagnetic energy term. The third term in Eq. (6), the Zeeman term, does not affect s-state excitons[17] and is omitted in Eq. (10). If we treat the magnetic field as a perturbation for exciton states in the low-field limit and use the hydrogenic wave functions in Eq. (8), Eq. (10) gives a diamagnetic shift of

$$\Delta E_r=3e^2\lambda^2B^2/16\mu \quad \text{(low-field limit)}, \quad (11)$$

which is proportional to the square of the magnetic field.

To include the effect of nonparabolic band dispersion in the calculation of the exciton resonance energy, we replace the kinetic-energy term by the summation in $\mathbf{k}$ space as

$$\left\langle\psi_{\rm env}\left|-\frac{\hbar^2}{2m_i}\left(\frac{\partial^2}{\partial r^2}+\frac{1}{r}\frac{\partial}{\partial r}\right)\right|\psi_{\rm env}\right\rangle$$
$$=\sum_{\mathbf{k}_\parallel}E_{i,n}^{\parallel}(\mathbf{k}_\parallel)|A_n(\mathbf{k}_\parallel)|^2 \quad (i=e,h), \quad (12)$$

where $E_{e,n}^{\parallel}(\mathbf{k}_\parallel)$ is the in-plane dispersion in the conduction band and $E_{h,n}^{\parallel}(\mathbf{k}_\parallel)$ is that in the valence band. We can then obtain the in-plane electron and hole effective masses from Eq. (12), and thus, the reduced effective mass of excitons for a given band dispersion. E_r can be calculated as a function of the magnetic field by Eq. (10).

In-plane conduction-band nonparabolic dispersion originates primarily from the first-order direct $\mathbf{k}\cdot\mathbf{p}$ interactions between s- and p-state eight band-edge bases.[20,26] Due to the upward shift of electron energy under quantum confinement, the in-plane effective mass at each subband increases as the well width decreases. According to Bastard, Brum, and Ferreira,[26] we calculated conduction-band energy

$$E_{e,n}=E_{e,n}^{z}+E_{e,n}^{\parallel}(\mathbf{k}_\parallel) \quad (13)$$

from the mass at the bulk band edge m_{Γ_6}.

To describe valence-band dispersion, it is well known that second-order indirect $\mathbf{k}\cdot\mathbf{p}$ coupling must be taken into account.[19–21] Since in $In_{0.53}Ga_{0.47}As$ excitons' hole energies are a few meV, much smaller than the zone-center spin-orbit splitting energy of about 350 meV,[27] we use the Luttinger-Kohn 4×4 Hamiltonian matrix[21] formed by the top-most HH and LH valence-band edge bases, i.e., $|\frac{3}{2},\pm\frac{3}{2}\rangle$ and $|\frac{3}{2},\pm\frac{1}{2}\rangle$. The effective-mass equation of (001) quantum wells is given by

$$[H_{\rm LK}+V(z)I_{4\times4}]\varphi_{4\times1}=E_{h,n}\varphi_{4\times1}, \quad (14)$$

where

$$E_{h,n}=E_{h,n}^{z}+E_{h,n}^{\parallel}(\mathbf{k}_\parallel), \quad (15)$$

$H_{\rm LK}$ is the 4×4 matrix including Luttinger-Kohn effective-mass parameters (γ_1, γ_2, and γ_3), $V(z)$ is confinement potential for degenerate HH and LH states, $I_{4\times4}$ is the 4×4 unit matrix, and $\varphi_{4\times1}$ is a row vector with $\varphi_{h,n}^{j}(z,\mathbf{k}_\parallel)$ as components. Since, at $\mathbf{k}_\parallel=0$, the nondiagonal terms in Eq. (14) disappear, each subband-edge energy and confined-state wave function can be calculated only by the diagonal terms. At points away from the zone center, the increasing nondiagonal terms mix the subband states, making dispersion very complicated.[28]

The 4×4 Hamiltonian can be separated into two equivalent 2×2 Hamiltonians by a unitary transformation.[29,30] We calculated valence-subband dispersion by numerically diagonalizing the $\mathbf{k}_\parallel$-dependent 2×2 matrix using the differential method under the following approximations. First, we let $\gamma_2=\gamma_3=\bar{\gamma}$ for all matrix elements. This corresponds to neglecting warping and assuming completely spherical dispersion in the bulk valence band. The dispersion calculated under such a spherical approximation or axial approximation (neglecting only in-plane anisotropy) keeps essential band structures under intersubband mixing.[29–32] Second, we use common Luttinger-Kohn parameters in both well and barrier layers. This is also a good approximation in type-I quantum wells, such as $In_{0.53}Ga_{0.47}As/InP$, as long as well and barrier layers are relatively thick and eigenstates are well localized in well layers. By the latter approximation, boundary conditions[33] that $\varphi_{2\times1}$ and $\Pi_{2\times2}\varphi_{2\times1}$ are continuous at interfaces are automatically satisfied in the differential method, where $\varphi_{2\times1}$ is a row vector for transformed bases and $\Pi_{2\times2}$ is the matrix obtained by integrating the unitary-transformed Luttinger-Kohn Hamiltonian across the interfaces. In Sec. IV, γ_1 and $\bar{\gamma}$ are determined to explain measured HH-LH splitting energies and the ground-state electron-HH exciton diamagnetic shifts.

B. Oscillator strength

Based on time-dependent perturbation theory, the integrated intensity of one-photon optical-absorption spectra of exciton resonance in quantum wells is written as[14,16,18,34]

$$S=\frac{\pi e^2\hbar}{cn_r\varepsilon_0 m_0}f \quad (16)$$

using the oscillator strength of

$$f=\frac{1}{m_0E_{\rm ex}D}\left|\sum_{\mathbf{k}_\parallel}A(\mathbf{k}_\parallel)P_{cv}(\mathbf{e},\mathbf{k}_\parallel)\right|^2, \quad (17)$$

where c is the speed of light, n_r is the refractive index, ε_0

is the permittivity of a vacuum, and $P_{cv}(\mathbf{e},\mathbf{k}_\parallel)$ is the transition-matrix element.

Using Eqs. (2) and (3), the transition matrix for the interband optical transition is given as

$$P_{cv}(\mathbf{e},\mathbf{k}_\parallel)=\sum_{i,j}\langle u^i_{c,0}|\mathbf{e}\cdot\mathbf{p}|u^j_{v,0}\rangle \times\langle\varphi^i_{e,n}(z,\mathbf{k}_\parallel)\varphi^j_{h,n}(z,\mathbf{k}_\parallel)\rangle \quad (18)$$

Neglecting interband mixing, Eq. (18) reduces to

$$P_{cv}(\mathbf{e},\mathbf{k}_\parallel)=\langle u_{c,0}|\mathbf{e}\cdot\mathbf{p}|u_{v,0}\rangle\langle\varphi_{e,n}|\varphi_{h,n}\rangle =M_{\mathrm{QW}}(\mathbf{e},\mathbf{k}_\parallel)M\langle\varphi_{e,n}|\varphi_{h,n}\rangle \quad (19)$$

For electron-HH exciton transitions under TE-mode incident light, i.e., the polarization vector $\mathbf{e}$ is perpendicular to the z direction, the polarization- and wave-vector-dependent term M_{QW} is given as[35]

$$M_{\mathrm{QW}}(\mathbf{e},\mathbf{k}_\parallel)=\frac{\sqrt{3(1+\cos^2\theta)}}{2}\quad(\mathbf{e}\perp z)\,, \quad (20)$$

where $\cos\theta=k_z/\sqrt{k_z^2+k_\parallel^2}$ and we take $k_z=n\pi/L_W$. On the basis of the $\mathbf{k}\cdot\mathbf{p}$ perturbation approach,[19] the transition-matrix element in bulk materials M is given as[36]

$$M^2=m_0^2P^2/6 =\frac{m_0^2}{12}\left[\frac{1}{m_{\Gamma_6}}-\frac{1+D'}{m_0}\right]\frac{E_A(E_A+\Delta_A)}{E_A+2\Delta_A/3}\,, \quad (21)$$

where P is the momentum matrix element between the s- and p-state function defined as $P=\langle S|p_j|j\rangle/m_0$ ($j=X$, Y, and Z), Δ_A is the spin-orbit splitting energy of well materials, and D' is the contribution of the second-order $\mathbf{k}\cdot\mathbf{p}$ perturbation. In Eq. (21), D' is often neglected.[36] In Sec. IV we will show that we should take into account D' to properly explain the integrated intensity of exciton resonance spectra.

If we neglect the wave-vector dependence of the transition-matrix element and substitute $M_{\mathrm{QW}}(\mathbf{e},0)$ at any $\mathbf{k}_\parallel$, the summation in $\mathbf{k}_\parallel$ space in Eq. (17) can be done analytically. Then, using the real-space wave function, Eq. (17) becomes

$$f=\frac{2P_{cv}^2(\mathbf{e},0)}{m_0E_{\mathrm{ex}}}|\phi_{\mathrm{ex}}(0)|^2\,, \quad (22)$$

where the factor of 2 represents the degeneracy due to spin. The oscillator strength is proportional to the probability of finding an electron and a hole at the same site.[22,23]

III. EXPERIMENTS

We grew three multiple quantum wells with $In_{0.53}Ga_{0.47}As$ well layers and InP barrier layers on (001) InP substrates by metal-organic vapor-phase epitaxy. The number of well layers is 20. The growth temperature was about 600 °C. First, we grew a 100-nm undoped InP buffer layer on an InP substrate, and then formed the multiple quantum wells. The background electron concentration is around 1×10^{15} cm^{-3}. The In, Ga, As, and P sources were trimethyleindium, triethylegallium, arsine, and phosphine. The carrier gas was Pd-diffused high-purity hydrogen, and the growth rate was about one monolayer per second.

The well and barrier layer thicknesses, L_w and L_B, were determined by transmission electron microscopy. Using the lattice image of InP layers to calibrate the scale, we measured and averaged the thickness of each layer. The composition of $In_{1-x}Ga_xAs$ well layers was exactly determined from the (004) x-ray diffraction angle of quantum wells using the composition dependence of the stiffness and lattice constants. The thickness and the composition of the three samples are (i) $L_w=13.6$ nm, $L_B=9.5$ nm, and $x=0.463$, (ii) $L_w=10.0$ nm, $L_B=9.6$ nm, and $x=0.467$, and (iii) $L_w=6.3$ nm, $L_B=9.4$ nm, and $x=0.465$. Since the lattice-matching condition to InP is $x=0.468$, these samples are lattice matched within 0.1% and we write the composition as $In_{0.53}Ga_{0.47}As$. Strictly speaking, however, the slight lattice mismatch is accommodated as a homogeneous tetragonal distortion and these samples receive biaxial compression. This biaxial strain is expected to split HH and LH band edges[37] by 1.6 meV in 6.3-nm, 0.6 meV in 10.0 nm, and 2.5 meV in 13.6-nm quantum wells (Table I), and is considered in the analysis below.

Magnetic fields of up to 8 T were applied perpendicularly to the sample using a split-coil superconducting magnet immersed in pumped liquid helium. A beam from a halogen lamp dispersed by a 0.32-m single-pass monochromator was focused onto the sample. The light transmitted through the sample was detected by a PbS detector using a conventional lock-in technique. The polarization vector is parallel to the quantum-well layers. The ratio between the light intensity transmitted from a sample I_1 and an InP substrate I_2 was normalized to one at an energy below the absorption edge. The optical absorbance of one quantum well was determined by

TABLE I. Well width L_w, barrier width L_B, composition x of $In_{1-x}Ga_xAs$ wells, splitting energies between 1e-hh and 1e-lh exciton resonances ΔE_{hl}, and the calculated strain contribution to the splitting $\Delta E_{\mathrm{strain}}$.

Sample	L_w (nm)	L_B (nm)	x	ΔE_{hl} (meV)	$\Delta E_{\mathrm{strain}}$ (meV)
I	13.6	9.5	0.463	14	2.5
II	10.0	9.6	0.467	22	0.6
III	6.3	9.4	0.465	51±3	1.6

$\alpha L_{QW}=(1/N)\ln(I_2/I_1)$, where N is the number of wells and $L_{QW}=L_w+L_B$.

Material parameters used in the calculations[27] are $\varepsilon=13.9\varepsilon_0$, $E_A=0.75$ eV, $E_B=1.35$ eV, $\Delta_A=0.37$ eV, $\Delta_B=0.1$ eV, $V_s=0.24$ eV, $V_p=-0.36$ eV, $V_\delta=-0.09$ eV, $m_{\Gamma_6}=0.044m_0$, and $n_r=3.5$. Here E_A and E_B are the band gaps, Δ_A and Δ_B are the spin-orbit splitting energies, A indicates well material, B indicates barrier materials, V_s is the conduction-band offset, V_p is the offset of valence-band maximum, and V_δ is the offset of the split-off band. According to Bastard, Brum, and Ferreira,[26] the signs of V_s, V_p, and V_δ are positive when the band-edge energy of each is higher in the barrier materials, i.e., $V_s>0$, $V_p<0$, and $V_\delta<0$ in type-I quantum wells. We assumed that 40% of the band-gap difference between InP and $In_{0.53}Ga_{0.47}As$ is in the conduction band.[38] Lawaetz calculated Luttinger-Kohn parameters for a wide variety of III-V and II-VI semiconductors.[39] From Table II of Ref. 39, we see $\gamma_1=19.67$, $\gamma_2=8.37$, and $\gamma_3=9.29$ in InAs and $\gamma_1=7.65$, $\gamma_2=2.41$, and $\gamma_3=3.28$ in GaAs, giving $\gamma_1=14.0$, $\gamma_2=5.57$, $\gamma_3=6.46$, and $\bar{\gamma}=(\gamma_2+\gamma_3)/2=6.02$ in $In_{0.53}Ga_{0.47}As$ from linear interpolation. These parameters, however, have not been tested experimentally and their uncertainty casts doubt on the calculated dispersion. We will determine a set of Luttinger-Kohn parameters, γ_1 and $\bar{\gamma}$, to properly explain magneto-optical data.

VI. MAGNETO-OPTICAL ABSORPTION IN $In_{0.53}Ga_{0.47}As$/InP QUANTUM WELLS

A. Optical-absorption spectra

Optical-absorption spectra of the quantum wells (Fig. 1) show that the electron-HH exciton resonance (1e-hh) spectrum is at the absorption edge and that the electron-LH resonance (1e-lh) is on the absorption continuum at shorter wavelengths for each quantum well. Due to the quantum confinement effect, the splitting energies between 1e-hh and 1e-lh resonances, ΔE_{hl}, increase as the well width decreases, and are 14 meV in 13.6-nm, 22 meV in 10.0-nm, and 51±3 meV in 6.3-nm quantum wells (Table I). Higher-order electron-HH exciton resonances, assigned as 2e-hh and 3e-hh, are also observed.

Figure 2 shows the magneto-optical absorption spectra of the quantum wells. Spectra of 1e-hh resonances show broadening with a full width at half maximum of 4.2 meV in 13.6-nm, 4.3 meV in 10.0-nm, and 9.4 meV in 6.3-nm quantum wells at zero fields. This low-temperature broadening is an inhomogeneous one primarily due to composition fluctuations and interface roughness.[16,40] The width depends little on the magnetic field; 4.2 meV (at 7 T) in 13.6-nm, 5.3 meV (6.2 T) in 10.0-nm, and 8.6 meV (7 T) in 6.3-nm quantum wells and spin-induced splitting of the exciton resonances was not observed in the measured field. In each quantum well, the 1e-hh exciton resonance at the absorption edge shows diamagnetic shifts and its intensity remarkably increases. The absorption continuum separates into discrete spectra, which are assigned as 2S and 3S states of 1e-hh excitons and are expected to approach Landau states in the high-field limit.[1] The 1e-lh exciton resonances merged into the electron-HH exciton resonances because of their weak oscillator strength and could not be detected under magnetic fields. We measured the diamagnetic shifts and integrated intensity of the ground-state (1S) 1e-hh exciton resonances as a function of the magnetic field. Taking the peak of the spectra as the resonance energy and using the low-energy side of the spectra, we extracted the contribution of the 1e-hh exciton resonance.

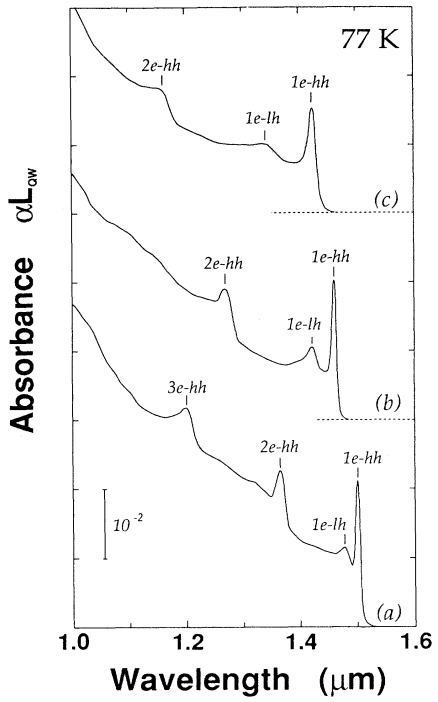

FIG. 1. Optical-absorption spectra at 77 K of $In_{0.53}Ga_{0.47}As$/InP quantum wells with well widths of (a) 13.6 nm, (b) 10.0 nm, and (c) 6.3 nm.

B. Diamagnetic shift

Diamagnetic shifts up to about 4–5 meV are observed in the measured field region (Fig. 3). While diamagnetic shifts in 13.6-nm and 10.0-nm quantum wells are almost identical, those in 6.3-nm quantum wells are definitely smaller. The lines on the measured values are calculated by Eq. (10) including both conduction- and valence-band nonparabolicity through Eq. (12). The calculations explain the measured shifts quite well up to 7–8 T.

The Luttinger-Kohn parameters, γ_1 and $\bar{\gamma}$, were determined by the following procedure. First, we calculated the valence-subband edge energies using Eq. (14) with $\mathbf{k}_\parallel=\mathbf{0}$ and we find sets of γ_1 and $\bar{\gamma}$ which give the measured splitting energy between the 1e-lh and 1e-hh resonances. We subtracted the contribution of the biaxial compression listed in Table I from the measured splitting energies, and neglected differences in the exciton binding energies between the two resonances. Then, we found a unique set that describes the 1e-hh diamagnetic shifts.

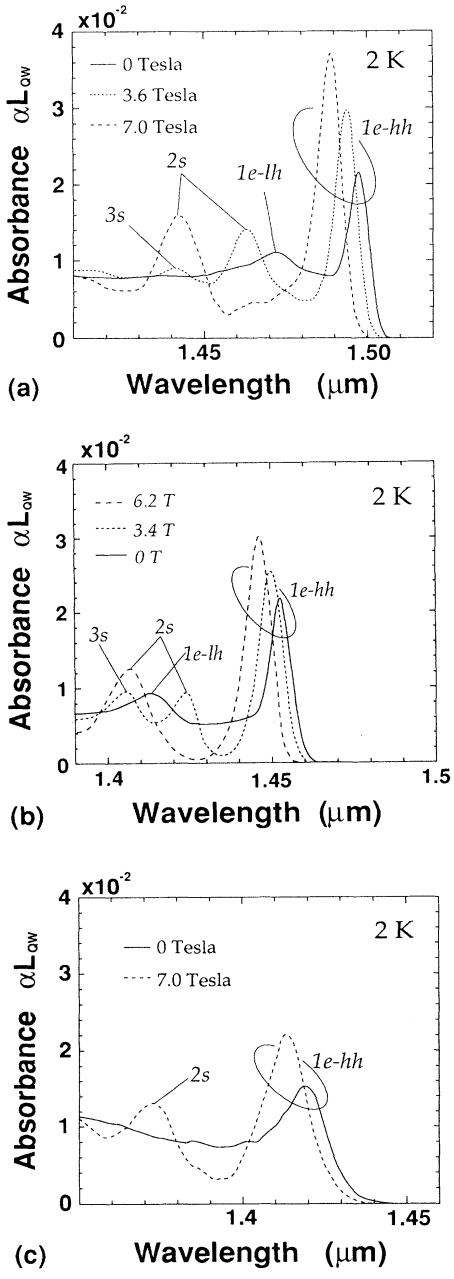

FIG. 2. Magneto-optical absorption spectra at 2 K of $In_{0.53}Ga_{0.47}As/InP$ quantum wells with well width of (a) 13.6 nm, (b) 10.0 nm, and (c) 6.3 nm. The magnetic field is perpendicular to the quantum-well layers.

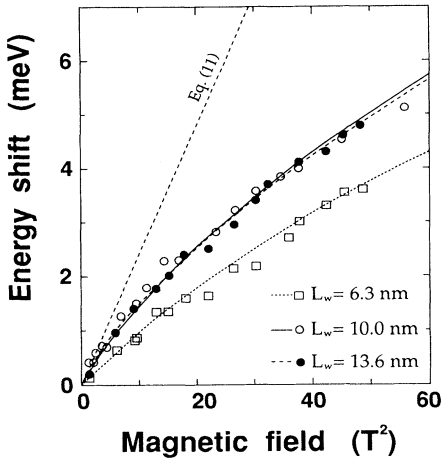

FIG. 3. Diamagnetic shift of the ground-state electron-HH exciton resonance spectra as a function of the square of the magnetic field. Luttinger-Kohn parameters were $\gamma_1=5.8$ and $\bar{\gamma}=2.0$ in 13.6-nm quantum wells, $\gamma_1=8.1$ and $\bar{\gamma}=2.4$ in 10.0-nm quantum wells, and $\gamma_1=6.3$ and $\bar{\gamma}=2.5$ in 6.3-nm quantum wells.

The in-plane reduced effective mass and in-plane effective masses of electrons and holes at zero field calculated by Eq. (12) are shown in Table II. Values of E_r at zero field, i.e., exciton binding energy E_b and the exciton radius λ, calculated by the hydrogenic wave function in Eq. (8), are also shown. These effective masses and Luttinger-Kohn parameters are discussed in Sec. IV D.

The dashed straight line, for 13.6-nm quantum wells, is the diamagnetic shift calculated by Eq. (11) in the low-field limit. The approximation of the low-field limit holds at most up to 1 or 2 T. Diamagnetic shifts under higher magnetic fields are no longer proportional to the square of the magnetic field and gradually bend away from the straight lines, showing that the in-plane exciton wave function shrinks (λ decreases) in the magnetic field.

To illustrate the dependence of exciton wave functions on the magnetic field, we show (a) $|\phi_{ex}(r)|^2$ and (b) $D^{1/2}k_{\parallel}A(k_{\parallel})$ under magnetic fields of 0, 4, and 8 T for 13.6-nm quantum wells (Fig. 4). These terms are closely related to the integrated intensity [Eqs. (17) and (22)]. We used variational parameters which explain diamagnetic shifts in Fig. 3; $a=0.8$, $b=0.203$, $\lambda=15.4$ nm, and $\eta=23.8$ nm at 0 T, $a=0.5$, $b=0.507$, $\lambda=10.2$ nm, and $\eta=20.0$ nm at 4 T, and $a=0.3$, $b=0.715$, $\lambda=6.6$ nm, and $\eta=16.2$ nm at 8 T. As the magnetic field increases,

TABLE II. Parameters of excitons at zero field. In-plane reduced effective mass $\mu^{\parallel}$, in-plane electron effective mass $m_e^{\parallel}$, in-plane HH effective mass $m_{hh}^{\parallel}$, binding energy E_b, and in-plane radius λ. Effective masses are in units of m_0.

Sample	$\mu^{\parallel}$	$m_e^{\parallel}$	$m_{hh}^{\parallel}$	E_b (meV)	λ (nm)
I	0.037	0.048	0.15	−5.8	16.4
II	0.035	0.05	0.12	−6.1	16.0
III	0.04	0.054	0.16	−7.3	13.2

the exciton wave function for in-plane relative motion shrinks and its amplitude at $r=0$, $\phi_{ex}(0)$, increases. This is due to the parabolic confinement potential proportional to the square of the magnetic field in the quantum-well plane [Eq. (10)]. To the contrary, the expansion coefficient $A(k_\parallel)$, which is the Fourier transform of the real-space wave function, extends in **k** space, increasing the area of $D^{1/2}k_\parallel A(k_\parallel)$. $D^{1/2}k_\parallel A(k_\parallel)$ peaks at $k_\parallel=0.054$ nm^{-1} at 0 T, $k_\parallel=0.071$ nm^{-1} at 4 T, and $k_\parallel=0.095$ nm^{-1} at 8 T, showing that excitons are formed mainly from states around these points. These wave vectors correspond approximately to the inverse of the radius of the real-space wave function. The magnetic field shrinks the exciton relative-motion wave function in the quantum-well plane and extends the expansion coefficients in **k** space, thus more states take part in the formation of excitons than under zero field.

Previously,[14] we could not explain the diamagnetic shifts in 10.0-nm quantum wells over the entire range of magnetic fields, due to the assumed parabolic bands. Comparing the measured and calculated diamagnetic shifts, the reduced effective mass of excitons increased under the field (Fig. 4 in Ref. 14). By taking into account band nonparabolicity here, the mass increased by a few percent under the magnetic field due to the extension of the expansion coefficient over nonparabolic bands. This results in the excellent agreements with the measured shifts in Fig. 3.

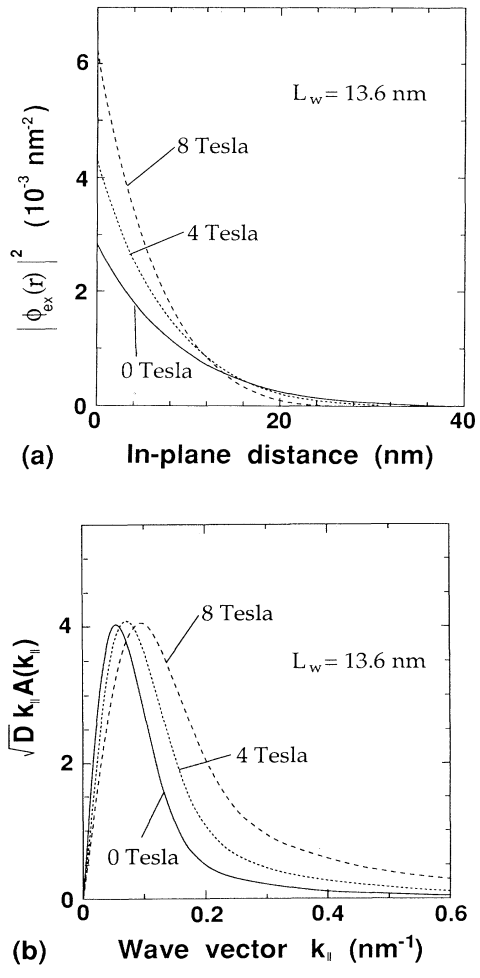

FIG. 4. (a) $|\phi_{ex}(r)|^2$ and (b) $D^{1/2}k_\parallel A(k_\parallel)$ for 13.6-nm quantum wells under magnetic fields perpendicular to quantum-well layers of 0, 4, and 8 T.

C. Oscillator strength

The integrated intensity increases monotonously with the magnetic field and shows about 50% enhancement around 7 T in each sample (Fig. 5). The intensity in 6.3-nm quantum wells is larger than that in 10.0- and 13.6-nm quantum wells. Lines were calculated by Eqs. (16) and (17) integrating the product of the expansion coefficient and the wave-vector-dependent matrix element in **k** space. We used variational parameters of Eq. (8) obtained from the diamagnetic shifts. We used D' in Eq. (21) as a fitting parameter and obtained $D'=-7$ for 13.6-nm quantum wells, $D'=-5$ for 10.0-nm quantum wells, and $D'=-6$ for 6.3-nm quantum wells. Note that D' is almost common in the three quantum wells. Using the average of $D'=-6$, we obtain the matrix element in Eq. (21) as $m_0P^2=11.5$ eV. This value is about 1.2 times larger than that calculated by neglecting D'.

By introducing the second-order **k**·**p** term on the matrix element, Eqs. (16) and (17) perfectly describe the measured integrated intensity of exciton resonance from zero field, at least into the intermediate-field region of 7–8 T. The enhancement of the integrated intensity, and thus oscillator strength, is due to the field-induced shrinkage of the exciton in-plane relative-motion wave function. Our previous analyses could not explain the integrated intensity over the entire field range (Fig. 4 in Ref. 14), partly due to the underestimates of the transition-matrix element and partly due to the assumed parabolic bands.

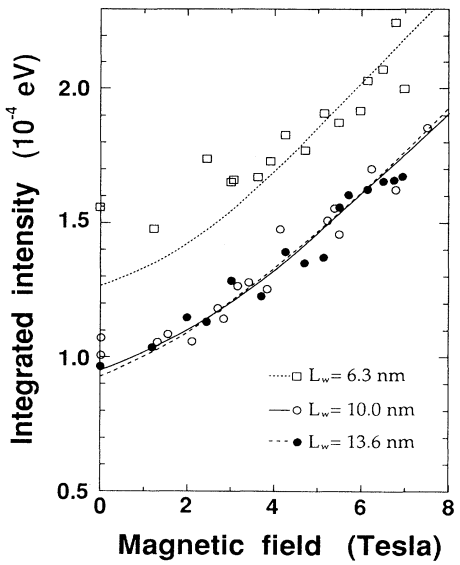

FIG. 5. Integrated intensity of the ground-state electron-HH exciton resonance spectra as a function of the magnetic field.

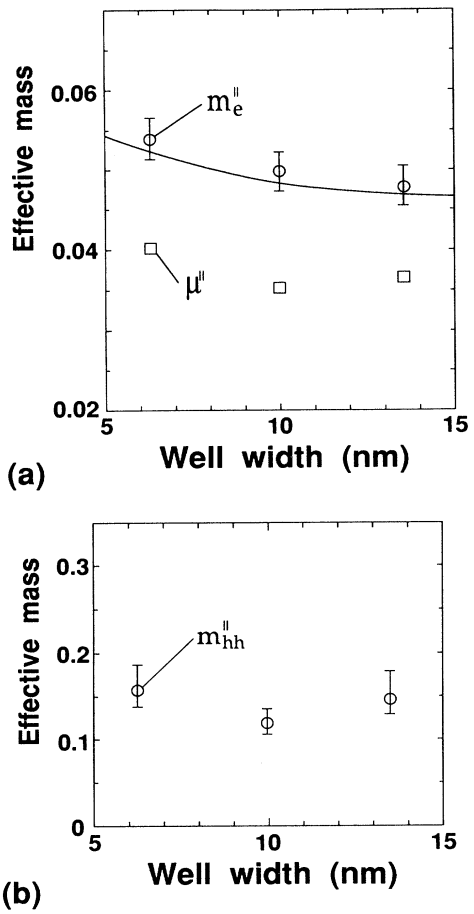

FIG. 6. (a) In-plane electron and reduced effective masses of excitons under zero field. The solid line represents the conduction-band-edge effective mass calculated using Bastard's formula (Ref. 26). (b) In-plane HH effective masses of excitons under zero field.

D. Effective-mass parameters

The effective masses we obtained are shown in Fig. 6. The solid line [Fig. 6(a)] represents the band-edge electron effective mass obtained by the second derivative of $E_{c,n}^{\parallel}(k_{\parallel})$ [Eq. (13)]. The electron effective mass increases as the well width decreases from the bulk band-edge mass of $0.044m_0$. This is due to the nonparabolic characteristics of the conduction band under the first-order $\mathbf{k}\cdot\mathbf{p}$ coupling.[26] Note that the electron effective mass of excitons is a few percent larger than the quantum-well band-edge mass due to the extension of the exciton expansion coefficient in $\mathbf{k}_{\parallel}$ space in the nonparabolic band. The masses increased further by a few percent under magnetic field due to the further extension of the expansion coefficient [Fig. 4(b)]. The reduced effective mass in the 6.3-nm quantum well is slightly larger than those in other thicker quantum wells, primarily due to the larger electron effective mass. In Fig. 6(b) we plotted the in-plane HH effective mass of excitons with error bars corresponding to the $\pm 5\%$ uncertainty in the calculated electron effective mass. Note that, though diagonal terms of the Luttinger-Kohn Hamiltonian give the band-edge HH effective mass as $(\gamma_1+\bar{\gamma})^{-1}$, the plotted masses are 10–30 % larger than the band-edge mass due to the nonparabolic characteristics of the valence band. Nonparabolic characteristics are more remarkable in the valence band than in the conduction band.

Luttinger-Kohn parameters obtained for the three samples were $\gamma_1=5.8$ and $\bar{\gamma}=2.0$ in 13.6-nm quantum wells, $\gamma_1=8.1$ and $\bar{\gamma}=2.4$ in 10.0-nm quantum wells, and $\gamma_1=6.3$ and $\bar{\gamma}=2.5$ in 6.3-nm quantum wells. If we assume $\pm 5\%$ error in the calculated electron effective mass, uncertainties of about ± 1 in γ_1 and ± 0.1 in $\bar{\gamma}$ are expected. We cannot discuss the well width dependence of Luttinger parameters due to these uncertainties. The averages of the parameters for the three samples are $\gamma_1=6.7$ and $\bar{\gamma}=2.3$. These values give a reasonable bulk valence-band effective mass[41] of $In_{0.53}Ga_{0.47}As$ as $m_0/(\gamma_1-2\bar{\gamma})=0.48m_0$ for the HH band and $m_0/(\gamma_1+2\bar{\gamma})=0.088m_0$ for the LH band. Note that our values are much smaller than $\gamma_1=14.0$ and $\bar{\gamma}=6.02$ obtained from Lawaetz's calculation[39] for $In_{0.53}Ga_{0.47}As$. The almost half values obtained in this work give about twice the in-plane HH mass at the band edge given by $m_0/(\gamma_1+\bar{\gamma})$. The calculated in-plane valence-band dispersion is strongly modified through the change in the degree of intersubband mixing, which depends on the HH-LH splitting energies and the magnitude of nondiagonal terms. To calculate Luttinger-Kohn parameters, we need the interband momentum matrix elements and energy separations between valence-band edges and remote even-parity band edges. The uncertainties in these quantities, which can hardly be obtained experimentally, may explain the discrepancy between Lawaetz's calculations and our values.

V. CONCLUSION

We studied diamagnetic shifts and the integrated intensity of exciton optical-absorption spectra in lattice-matched $In_{0.53}Ga_{0.47}As/InP$ quantum wells under magnetic fields perpendicular to quantum-well layers. We observed both diamagnetic shifts and the enhancement of integrated intensity in the ground-state electron-HH exciton resonance under magnetic fields of up to 8 T at 2 K. We demonstrated that the integrated intensity enhancement, and thus the oscillator strength of exciton transitions, is due to the field-induced shrinkage of the excitons in quantum-well planes or, equivalently, their field-induced extension in $\mathbf{k}$ space. We evaluated in-plane electron, hole, and reduced effective masses of excitons, Luttinger-Kohn valence-band effective-mass parameters, and a momentum matrix element between s- and p-state band-edge basis functions.

[1]O. Akimoto and H. Hasegawa, J. Phys. Soc. Jpn. **22**, 181 (1967).

[2]N. Miura, Y. Iwasa, S. Tarucha, and H. Okamoto, in *Proceedings of the 17th International Conference on the Physics of Semiconductors*, edited by J. D. Chadi and W. A. Harrison (Springer, New York, 1984), p. 359.

[3]J. C. Maan, G. Belle, A. Fasolino, M. Altarelli, and K. Ploog, Phys. Rev. B **30**, 2253 (1984).

[4]S. Tarucha, H. Okamoto, Y. Iwasa, and N. Miura, Solid State Commun. **52**, 815 (1984).
[5]S. Tarucha, H. Iwamura, T. Saku, H. Okamoto, Y. Iwasa, and N. Miura, Surf. Sci. **174**, 194 (1986).
[6]D. C. Rogers, J. Singleton, R. J. Nicholas, C. T. Foxon, and K. Woodbridge, Phys. Rev. B **34**, 4002 (1986).
[7]W. Ossau, B. Jakel, E. Bangert, G. Landwehr, and G. Weimann, Surf. Sci. **174**, 188 (1986).
[8]D. J. Mowbray, J. Singleton, M. S. Skolnic, N. J. Pulsford, S. J. Bass, L. L. Taylor, R. J. Nicholas, and W. Hayes, Superlatt. Microstruct. **3**, 471 (1987).
[9]A. S. Plaut, J. Singleton, R. J. Nicholas, R. T. Harley, S. R. Andrews, and C. T. B. Foxon, Phys. Rev. B **38**, 1323 (1988).
[10]G. E. W. Bauer and T. Ando, Phys. Rev. B **38**, 6015 (1988).
[11]D. D. Smith, M. Dutta, X. C. Liu, A. F. Terzis, A. Petrou, M. W. Cole, and P. G. Newman, Surf. Sci. **228**, 184 (1990).
[12]R. J. Warburton, G. M. Sundaram, R. J. Nicholas, S. K. Haywood, G. J. Ress, N. J. Mason, and P. J. Walker, Surf. Sci. **228**, 270 (1990).
[13]X. L. Zheng, D. Heiman, and B. Lax, Phys. Rev. B **40**, 10 523 (1989).
[14]M. Sugawara, Phys. Rev. B **45**, 11 423 (1992).
[15]J. O. Dimmock, *Semiconductors and Semimetals* (Academic, New York, 1967), Vol. III, Chap. 7, p. 259.
[16]M. Sugawara, T. Fujii, S. Yamazaki, and K. Nakajima, Phys. Rev. B **42**, 9587 (1990).
[17]R. S. Knox, *Theory of Excitons* (Academic, New York, 1963).
[18]G. D. Sanders and Y.-C. Chang, Phys. Rev. B **35**, 1300 (1987).
[19]E. O. Kane, J. Phys. Chem. Solids **1**, 249 (1957).
[20]E. O. Kane, J. Phys. Chem. Solids **1**, 82 (1956).
[21]J. M. Luttinger and W. Kohn, Phys. Rev. **97**, 869 (1955).
[22]R. J. Elliott, Phys. Rev. **108**, 1384 (1957).
[23]M. Shinada and S. Sugano, J. Phys. Soc. Jpn. **21**, 1936 (1966).
[24]D. A. B. Miller, D. S. Chemla, T. C. Damen, A. C. Gossard, W. Wiegmann, T. H. Wood, and C. A. Barrus, Phys. Rev. B **32**, 1043 (1985).
[25]R. L. Greene and K. K. Bajaj, Phys. Rev. B **31**, 6498 (1985).
[26]G. Bastard, J. A. Brum, and R. Ferreira, in *Solid State Physics* (Academic, New York, 1991), Vol. 44, p. 229.
[27]H. Nagai, S. Adachi, and T. Fukui, *III-V Alloy Semiconductors* (in Japanese) (Corona Publishing, Tokyo, 1988).
[28]See the review article of E. P. O'Reilly, Semicond. Sci. Technol. **4**, 121 (1989).
[29]D. A. Brido and L. J. Sham, Phys. Rev. B **31**, 888 (1985).
[30]A. T. Twardowski and C. Herman, Phys. Rev. B **35**, 8144 (1987).
[31]M. Altarelli, U. Ekenberg, and A. Fasolino, Phys. Rev. B **32**, 5138 (1985).
[32]U. Ekenberg, L. C. Andreani, and A. Pasquarello, Phys. Rev. B **46**, 2625 (1992).
[33]G. Bastard and J. A. Brum, IEEE J. Quantum Electron. **QE-22**, 1625 (1986).
[34]W. T. Masselink, P. J. Pearah, J. Klem, C. K. Peng, H. Morkoc, G. D. Sanders, and Y.-C. Chang, Phys. Rev. B **32**, 8027 (1985).
[35]M. Yamanishi and I. Suemune, Jpn. J. Appl. Phys. **23**, L35 (1984).
[36]H. C. Casey and M. B. Panish, *Heterostructure Lasers* (Academic, New York, 1978), Chap. 3.
[37]F. H. Pollak, *Semiconductor and Semimetals* (Academic, New York, 1990), Vol. 32, Chap. 2.
[38]S. R. Forrest, P. H. Schmidt, R. B. Wilson, and M. L. Kaplan, Appl. Phys. Lett. **45**, 1199 (1984).
[39]P. Lawaetz, Phys. Rev. B **4**, 3460 (1971).
[40]M. Sugawara, T. Fujii, S. Yamazaki, and K. Nakajima, Phys. Rev. B **44**, 1782 (1991).
[41]M. Cardona, *Semiconductor and Semimetals* (Academic, New York, 1967), Vol. 3, Chap. 5, p. 151.